metals

MDPI

Article

Effects of Alloying Element on Hydrogen Adsorption and Diffusion on α-Fe(110) Surfaces: First Principles Study

Luying Zhang [1], Qingzhe Zhang [1], Peng Jiang [2,3,*], Ying Liu [1], Chen Zhao [1] and Yuhang Dong [1]

[1] School of Petroleum Engineering, Northeast Petroleum University, Daqing 163318, China; zhangluying@nepu.edu.cn (L.Z.); zhangqingzhe@stu.nepu.edu.cn (Q.Z.); liuying@stu.nepu.edu.cn (Y.L.); 238003020662@stu.nepu.edu.cn (C.Z.); 238003020658@stu.nepu.edu.cn (Y.D.)
[2] Sanya Offshore Oil & Gas Research Institute, Northeast Petroleum University, Sanya 572025, China
[3] School of Mechanical Science and Engineering, Northeast Petroleum University, Daqing 163318, China
* Correspondence: jiangpeng@nepu.edu.cn

Abstract: Based on first principles density functional theory (DFT) methods, this study employed the Cambridge Serial Total Energy Package (CASTEP) module within Materials Studio (MS) software under the generalized gradient approximation to investigate the adsorption, diffusion behavior, and electronic properties of hydrogen atoms on α-Fe(110) and α-Fe(110)-Me (Mn, Cr, Ni, Mo) surfaces, including calculations of their adsorption energies and density of states (DOS). The results demonstrated that doping with alloy atoms Me increased the physical adsorption energy of H_2 molecules on the surface. Specifically, Mo doping elevated the adsorption energy from −1.00825 eV to −0.70226 eV, with the largest relative change being 30.35%. After doping with Me, the chemical adsorption energy of two hydrogen atoms does not change significantly, among which doping with Cr results in a decrease in the chemical adsorption energy. Building on this, further analysis of the chemical adsorption of single atoms on the surface was conducted. By comparing the adsorption energy and the bond length between a hydrogen atom and iron/dopant metal atom, it was found that Mo doping has the greatest impact, increasing the bond length by 58.58%. Analysis of the DOS functions under different doping conditions validated the interaction between different alloy elements and H atoms. Simultaneously, simulations were carried out on the energy barrier crossed by H atoms diffusing into the metal interior. The results indicate that Ni doping facilitates the diffusion of H atoms, while Cr, Mn, and Mo hinder their diffusion, with Mo having the most significant effect, where its barrier is 21.88 times that of the undoped surface. This conclusion offers deep insights into the impact of different doping elements on hydrogen adsorption and diffusion, aiding in the design of materials resistant to hydrogen embrittlement.

Keywords: alloying element; α-Fe(110) surface; first principles; hydrogen adsorption; hydrogen diffusion

Citation: Zhang, L.; Zhang, Q.; Jiang, P.; Liu, Y.; Zhao, C.; Dong, Y. Effects of Alloying Element on Hydrogen Adsorption and Diffusion on α-Fe(110) Surfaces: First Principles Study. *Metals* **2024**, *14*, 487. https://doi.org/10.3390/met14050487

Academic Editor: Alain Pasturel

Received: 8 March 2024
Revised: 15 April 2024
Accepted: 19 April 2024
Published: 23 April 2024

1. Introduction

To effectively safeguard our environment and address the escalating depletion of traditional non-renewable energy sources such as coal, oil, and natural gas, hydrogen gas is emerging as a promising, pollution-free, and sustainable alternative. This renewable energy source is increasingly utilized across various sectors, particularly in electricity production, transportation, and domestic energy supply. Hydrogen energy exhibits its unique advantages in these fields, proving to be an efficient and environmentally friendly solution [1–3]. In an innovative approach to energy transportation, the use of existing natural gas pipelines for the conveyance of hydrogen gas is being explored as a method to save energy and reduce emissions. This method has significant development potential and has attracted global attention. Such an approach does not only make efficient use of the already established energy infrastructure, but also fosters the rapid expansion and application of hydrogen energy [4–7]. Various countries have begun to implement this strategy. For example, Germany has successfully utilized its pipelines to transport

hydrogen-doped natural gas, which has resulted in a reduction in hydrogen transmission costs by 60% [8]. However, the integration of hydrogen into the existing pipeline systems presents a notable challenge due to the material properties of pipeline steel. Pipeline steel exhibits a high sensitivity to hydrogen, a phenomenon well documented in the scientific literature [9,10]. Even minimal concentrations of hydrogen can lead to the embrittlement of metals and alloys. This embrittlement significantly diminishes their mechanical properties, thereby posing risks to the structural integrity and safety of the pipelines [11–13]. When hydrogen gas is transported through pipelines, it adsorbs and diffuses into the metal, altering the metal lattice structure. This change can severely impact the fracture toughness of the metal [14,15], effectively reducing the durability and operational lifespan of the pipeline, and causing serious or even catastrophic accidents [16–18].

The problem of a hydrogen-induced reduction in the mechanical properties of steel has been extensively studied [19,20]. So far, several hydrogen embrittlement (HE) mechanisms have been proposed, including the Hydrogen Pressure Theory [21], Weak Bond Theory (HEDE) [22], Reduced Surface Energy Theory [23], Promoted Local Plastic Deformation Theory (HELP) [24], and Plastic Deformation Suppression Theory [25], etc. However, current theories and research on hydrogen embrittlement predominantly aim to elucidate the specific mechanisms by which hydrogen induces embrittlement phenomena in materials. These theories provide a foundational understanding that, while effective to a degree, does not thoroughly encompass all the manifestations of hydrogen embrittlement observed under diverse conditions. Existing models often overlook the complex interplay between microstructural features and hydrogen interactions, which can vary significantly depending on the material and environmental conditions. This gap in knowledge suggests a pressing need for more comprehensive and detailed investigations into the mechanisms of hydrogen embrittlement. Such research would not only deepen our understanding of the fundamental impacts of hydrogen on material properties, but also enhance our ability to predict and mitigate the adverse effects of hydrogen in critical applications. Therefore, it is imperative to conduct further in-depth and extensive studies to uncover and fully comprehend the complete range of impact mechanisms exerted by hydrogen on various materials.

The entry of hydrogen into the interior of metals typically occurs in three stages. Firstly, hydrogen molecules physically adsorb onto the metal surface [26], and subsequently, they transition from physical adsorption to chemical adsorption [27,28]. At this point, hydrogen molecules dissociate into hydrogen atoms [29]. Finally, hydrogen atoms diffuse into the metal through the gaps in the metal lattice, migrating and accumulating at dislocations, vacancies, and the like, resulting in the phenomenon of metal hydrogen embrittlement. Therefore, studying the adsorption and diffusion processes of hydrogen atoms is fundamental to conducting research on hydrogen-induced cracking. For instance, Yu et al. utilized DFT and ab initio atomic thermodynamics to demonstrate that H_2 molecules tend to dissociate both dynamically and thermodynamically, and the stable coverage of hydrogen on the surface highly depends on temperature and H_2 partial pressure [30]. Álvarez-Falcón et al. investigated the adsorption and dissociation of hydrogen on copper surfaces and found that van der Waals forces play a crucial role in H_2 adsorption [31]. Yanachkov et al., through stress-relaxation tests and self-consistent kinetic Monte Carlo simulations conducted on pure iron, found that hydrogen charging alters dislocation migration, leading to an increased likelihood of dislocation cell structure formation in cold-rolled and annealed samples [32]. Zhang et al. employed a simulation study on the adsorption behavior of hydrogen atoms and H_2 on different crystallographic planes of FeO surfaces using DFT. They found that H_2 molecules tend to physically adsorb at the top positions of Fe atoms, while Fe atoms on the FeO surface act as active sites catalyzing the dissociation of H_2. The dissociated H atoms are more inclined to form chemical bonds with surface O atoms [33]. Dadfarnia et al. proposed a modified hydrogen transport model and concluded that dislocations contribute to increasing the local hydrogen concentration before crack initiation [34]. Ferrin et al. observed that the relative instability of hydrogen presents significant barriers to entry into transition metals, while the diffusion activation energy from the

first to the second surface is relatively low [35]. Xie et al. studied the adsorption structure of hydrogen molecules on the Fe(110) surface and found that an energy barrier crossing of 0.08 eV occurs at a distance of 2.3~2.5 Å from the surface, indicating the transition from physical adsorption to chemical adsorption [36]. Chohan et al. found that under hydrogen atom adsorption on the Fe surface, the distance between first-layer atoms and second-layer atoms increases, providing better diffusion space for H atoms. The interaction between hydrogen and the Fe(110) surface, followed by the subsequent adsorption of hydrogen on the surface, constitutes the first step in the mechanism of hydrogen embrittlement in ferritic steels, so it also represents an opportunity to delay or prevent the damage of these materials in hydrogen-rich environments [37].

However, hydrogen pipelines are not solely composed of a single metal. The doping of alloying elements such as Cr, Mn, Ni, and Mo in steel materials can improve the chemical and mechanical properties of the steel [38–42]. Extensive research has been conducted on the impact of these alloying elements on the mechanical properties of metals, with most studies examining their effects at the macroscopic level. These studies typically focus on how these elements improve the strength, ductility, and resistance to environmental degradation. However, while macroscopic investigations provide valuable insights, research at the molecular level is equally crucial but less extensive. At this scale, studies predominantly analyze the effects on the surfaces of single elements. This approach tends to overlook the synergistic or antagonistic impacts that a combination of multiple elements might have on material properties, particularly regarding the adsorption of hydrogen atoms. The interaction between hydrogen atoms and these complex alloy surfaces could potentially alter the adsorption characteristics significantly, yet the collective effects of multiple alloying elements on hydrogen adsorption remain underexplored. Liu et al. conducted first principles calculations to study the adsorption and diffusion behaviors of nitrogen atoms in titanium alloys, finding that the addition of aluminum atoms reduces the adsorption capacity of nitrogen atoms but significantly promotes the diffusion of nitrogen atoms inward, facilitating the formation of a deeper nitridation layer [43]. In this study, we draw upon the first principles calculation method used by Liu et al. to analyze the effects of alloying elements (Cr, Mn, Ni, Mo) on the adsorption of hydrogen on the α-Fe(110) surface in terms of adsorption energy and density of states, providing a theoretical basis for designing new materials resistant to hydrogen embrittlement.

2. Computational Methodology

All calculations in this paper were performed using the CASTEP [44] module, version 2020, which is based on first principles DFT within the MS molecular dynamics simulation software by Accelrys, San Diego, CA, USA. The most stable adsorption sites for hydrogen were determined through simulation. Models for hydrogen adsorption and hydrogen incorporation diffusion on α-Fe(110)-Me (Mn, Cr, Ni, Mo) surfaces doped with four different metal elements and undoped Fe(110) surfaces were established. The electron wave function is expanded by the plane wave basis vector. To reduce the plane wave basis set, this paper employed ultrasoft pseudopotential, and the electronic exchange-correlation energy adopted the Revised Perdew–Burke–Ernzerhof (RPBE) [45] functional within the generalized gradient approximation (GGA) [46]. The Broyden–Fletcher–Goldfarb–Shanno (BFGS) [47,48] algorithm is used for geometric optimization in the calculation process. At the same time, the linear synchronous transit quadratic synchronous transit (LST/QST) transition state search method was simultaneously employed to find the transition state, enabling the investigation of the energy required for adsorption and diffusion state transitions. Subsequently, their adsorption energy, DOS functions, and energy barrier crossing were compared and analyzed to discuss the effects of different elements on hydrogen adsorption and diffusion.

2.1. Site Selection

To delve into the adsorption stability of hydrogen on the Fe(110) surface, this study identified three main adsorption configurations based on potential adsorption sites for hydrogen atoms on metal surfaces: top site adsorption (Top, T), bridge site adsorption (Bridge, B), and three-fold hollow site adsorption (Threefold, TF), as illustrated in Figure 1a. Further simulations revealed four distinct adsorption positions for hydrogen atoms on the Fe(110) surface, namely T1, T2, B, and TF, with T1 and T2 both representing top site adsorptions but located at different atomic positions, as depicted in Figure 1b. This research conducted adsorption simulations for hydrogen at T1, T2, B, and TF sites on both α-Fe(110) and α-Fe(110) -Me (Mn, Cr, Ni, Mo) surfaces, comparing these to identify the most favorable adsorption site for hydrogen with enhanced credibility.

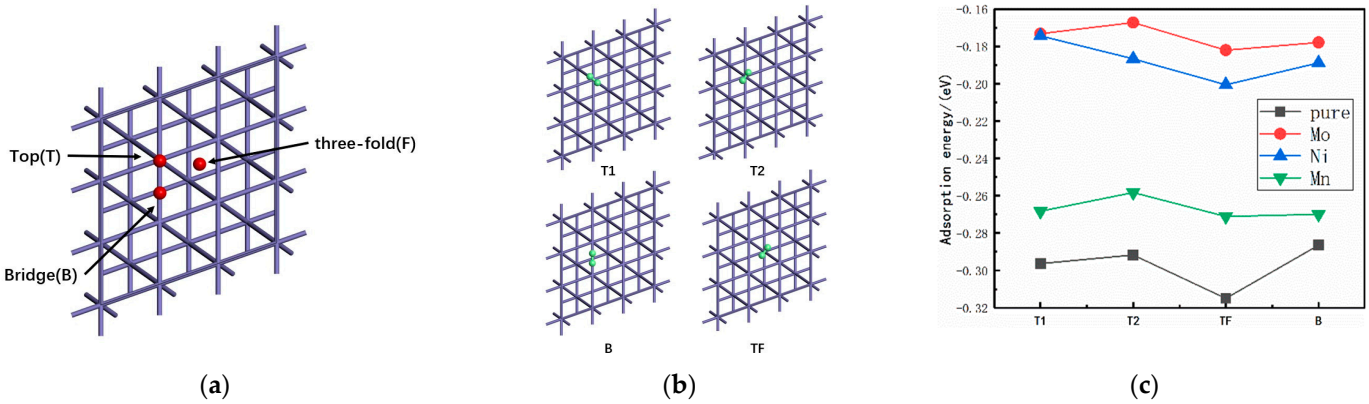

(**a**) (**b**) (**c**)

Figure 1. Adsorption configurations and energy profiles, (**a**) adsorption sites' representation, (**b**) adsorption positions, (**c**) adsorption energy profiles.

According to the simulation results shown in Figure 1c, hydrogen achieves optimal adsorption states at the TF site on both α-Fe(110) and α-Fe(110) -Me (Mn, Cr, Ni, Mo) surfaces, thereby selecting this site for the adsorption model established in the following sections.

2.2. Adsorption Model Construction

In the construction of the initial calculation model of the cell, the experimental lattice constants of the body-centered cubic structure of α-Fe provided by MS were used. Within MS, we established a cell characterized by lattice parameters of a = b = c = 2.8664 Å and $\alpha = \beta = \gamma = 90^{\circ}$. Subsequent geometric optimization was conducted, during which all atoms within the cell were allowed to fully relax in order to achieve the configuration of the lowest energy. To ensure the accuracy of the results, tests were conducted on the effects of energy cut-off and the k-point grid on the lattice constant before simulation. The results show that when the energy cut-off is 425 eV and the k-point grid is 15 × 15 × 15, the energy converges to the 5×10^{-6} eV/atom. The optimization results are shown in Figure 2b. The calculated lattice constant is 2.781 Å, which is in good agreement with the experimental value of 2.8664 Å, with an error of 2.9%, indicating that the calculation method and parameter settings used for structural optimization in this paper are reasonable.

While ensuring the accuracy of the calculations and minimizing the computational cost, this paper used the Cleave Surface function provided by MS to perform cutting surface treatment on the optimized unit cell and selected α-Fe(110) surface cutting modeling as the research object. A vacuum of 12 Å was added, and a 2 × 2 × 1 supercell was utilized. The resulting Fe(110) surface is displayed in Figure 2c. Hydrogen molecules were added at the three-fold hollow site to obtain the initial adsorption configuration. The atomic layers totaled three layers, with the bottom two layers fixed to simulate the bulk phase, while the topmost layer of atoms remained unfixed to simulate the surface and underwent free relaxation during geometric optimization. The stable adsorption positions were calculated using the CASTEP module to investigate the influence of different dopant atoms on the

surface adsorption of H_2 molecules. Subsequently, Fe atoms were replaced at specific positions to simulate doping, as depicted in Figure 2d.

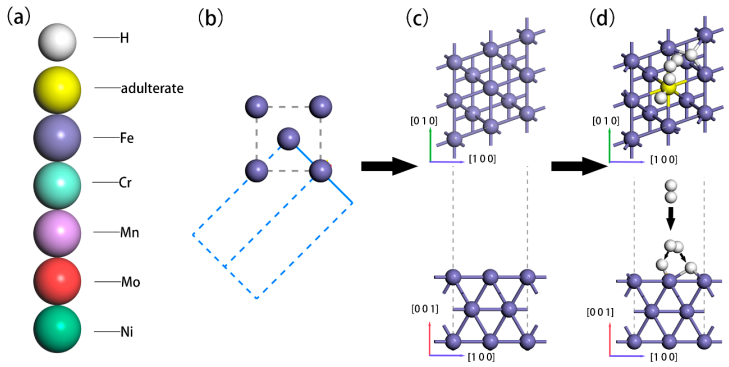

Figure 2. Hydrogen adsorption model, (**a**) each element model, (**b**) surface cutting position, (**c**) Fe(110) surface schematic diagram, (**d**) doping element position and H_2 molecular adsorption process.

2.3. Calculation of Adsorption Energy

To analyze the stability of hydrogen adsorption on the surface, we employed first principles methods based on DFT. We calculated two key metrics: the adsorption energy of a single hydrogen molecule (E_{ad1}) and the adsorption energy of the two hydrogen atoms after dissociation (E_{ad2}). These adsorption energies are critical indicators of the ease with which atoms or molecules can adsorb onto a surface. They are derived by calculating the energy difference between the systems before adsorption and after adsorption. A higher absolute value of the adsorption energy indicates a more stable adsorption. The larger the absolute value, the more stable the adsorption. The calculation formula is as shown in Formulas (1) and (2).

$$|E_{ad1}| = \left| E_{H_2/Fe-slab} - E_{Fe-slab} - E_{H_2} \right| \quad (1)$$

$$|E_{ad2}| = |E_{2H/Fe-slab} - E_{Fe-slab} - 2E_H| \quad (2)$$

where $E_{H_2/Fe-slab}$ represents the energy of the physical adsorption of the H_2 molecule on the surface, $E_{Fe-slab}$ represents the energy of the optimized Fe surface, E_{H_2} represents the energy of the isolated hydrogen molecule, $E_{2H/Fe-slab}$ represents the energy of the chemisorption of two hydrogen atoms, and E_H represents the energy of the isolated hydrogen atom.

To study the influence of doping with different elements on hydrogen adsorption, this study calculates the adsorption energies of individual hydrogen molecules (E_{ad3}) and two hydrogen atoms (E_{ad4}) on different doped surfaces.

$$|E_{ad3}| = \left|E_{H_2/Fe-x-slab} - E_{Fe-x-slab} - E_{H_2}\right| \quad (3)$$

$$|E_{ad4}| = |E_{2H/Fe-x-slab} - E_{Fe-x-slab} - 2E_H| \quad (4)$$

where x represents Fe, Cr, Mn, Ni, and Mo atoms; $E_{H_2/Fe-x-slab}$ represents the total system energy of hydrogen molecule chemisorption on the doped surface; $E_{2H/Fe-x-slab}$ represents the total energy of the system after the chemisorption of 2 H atoms; and $E_{Fe-x-slab}$ represents the total energy of the Fe(110) surface with a doping element before adsorption.

The Hirshfeld charge difference is obtained from Equation (5)

$$\Delta Q = |q_a - q_b| \quad (5)$$

q_a represents the Hirshfeld charge before adsorption, and q_b represents the Hirshfeld charge after adsorption.

2.4. Adsorption of Hydrogen on Metal Surface

H_2 adsorption undergoes a transition from physical adsorption to chemical adsorption. In this paper, stable physical adsorption and chemical adsorption positions were first identified using the CASTEP module. Then, the transition state was determined using the complete LST/QST method to investigate the energy barrier for the adsorption state transition. The construction of the model also utilized the RPBE functional under the GGA approximation in the CASTEP module, with a plane-wave energy cut-off of 450 eV and a k-point grid of 10 × 10 × 1 to ensure energy convergence to the 1×10^{-5} eV/atom, as shown in Figure 3.

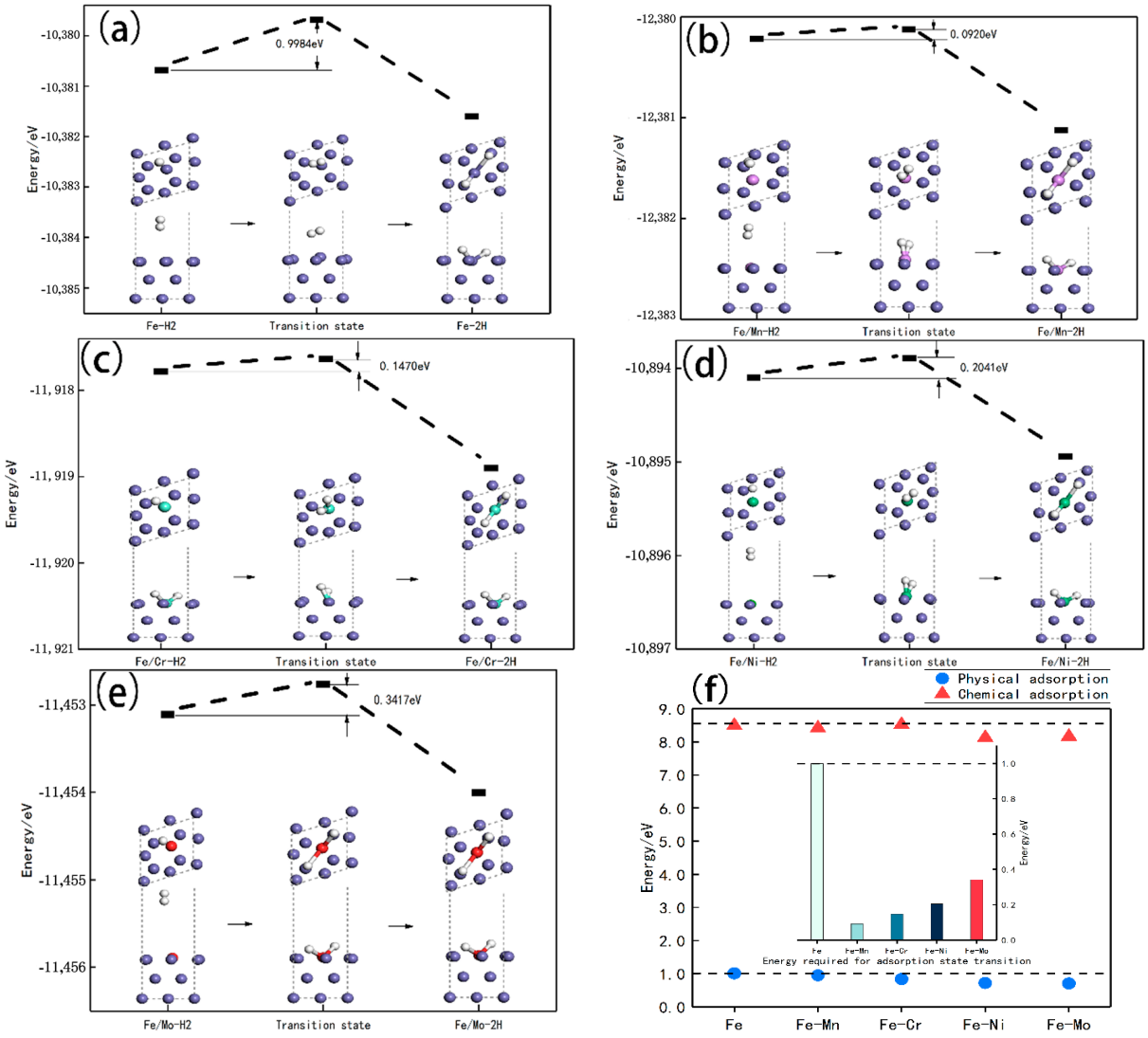

Figure 3. H_2 adsorption process on different alloy surfaces: (**a**) hydrogen adsorption on Fe surface, (**b**) hydrogen adsorption on Fe/Mn surface, (**c**) hydrogen adsorption on Fe/Cr surface, (**d**) hydrogen adsorption on Fe/Ni surface, (**e**) hydrogen adsorption on Fe/Mo surface, (**f**) energy barrier of physical adsorption energy, chemical adsorption energy, and adsorption state transition on each surface.

2.5. Adsorption and Diffusion of Hydrogen Atoms on the Metal Surface

To further study the effect of alloys on its adsorption, this study utilized the CASTEP module to simulate the adsorption and diffusion of single H atoms on the alloy surface. The model construction is shown in Figure 4a. The yellow atoms represent the positions where alloy elements are doped. We compute the adsorption energy, the bond length, charge transfer values, and DOS functions for different doping scenarios and compare them

with hydrogen adsorption on an undoped Fe(110) surface. This analysis aims to assess the impact of different alloy element doping on hydrogen adsorption. Additionally, we use the LST/QST method to find the energy barrier for adsorption and diffusion into the metal, determining their ease or difficulty.

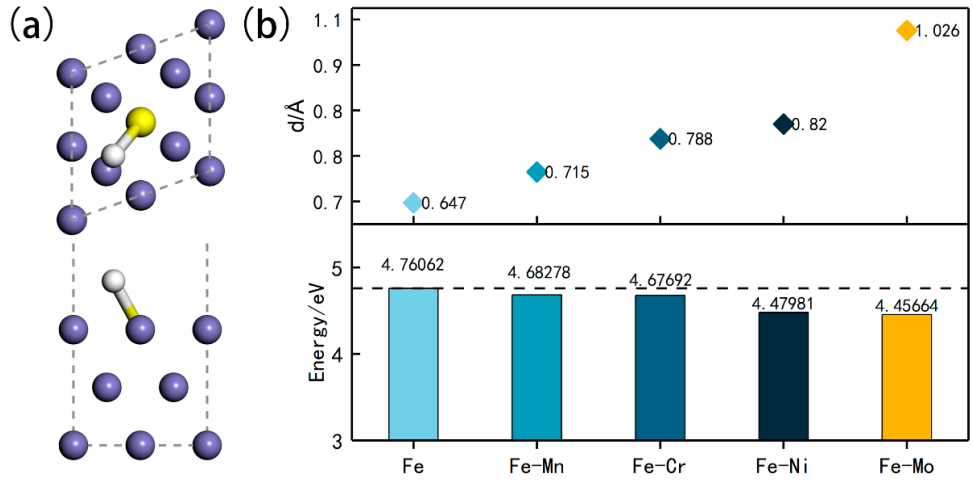

Figure 4. Chemisorption of a single H atom, (**a**) adsorption model, (**b**) absolute value of adsorption energy/bond length.

3. Results and Discussion

3.1. Hydrogen Adsorption under Different Doping

The absolute values of the adsorption energies for physical and chemical adsorption after alloy doping are shown in Table 1 and Figure 4, respectively. From Figure 4, it can be observed that the incorporation of alloy elements leads to a decrease in the energy required for the transition between adsorption states, making hydrogen more prone to transition from physical to chemical adsorption. Specifically, the doping of Mn, Cr, Ni, and Mo alloys reduces the stability of the physical adsorption of H_2 molecules, with the absolute values of the physical adsorption energies decreasing by 6.00%, 17.13%, 28.71%, and 30.35%, respectively, compared to the undoped surface. Regarding chemical adsorption energies, compared to the undoped surface, Mn, Ni, and Mo decrease by 0.89%, 4.27%, and 3.91%, respectively, while Cr increases by 0.36%.

Table 1. The value of physical adsorption energy, the energy barrier of adsorption state transition, and the absolute value of chemical adsorption energy.

Adsorption Surface	Physical Adsorption Energy (eV)	The Energy Required for Adsorption State Transition (eV)	Chemisorption Energy (eV)
Fe	−1.0083	0.9984	8.4872
Fe-Mn	−0.9478	0.0919	8.4117
Fe-Cr	−0.8355	0.1470	8.5174
Fe-Ni	−0.7188	0.2041	8.1252
Fe-Mo	−0.7023	0.3417	8.1557

3.2. Hydrogen Atom Chemisorption

It can be seen from Figure 4b that the bond lengths of the H atoms on the surfaces doped with Mn, Cr, Ni, and Mo are all increased compared to the pure iron surface. The respective increments are 10.51% for Mn, 21.97% for Cr, 26.74% for Ni, and 58.58% for Mo doping. Among them, doping with Mo has the greatest impact on the stability of chemical

adsorption, resulting in the greatest distance between the H atom and the surface, which is 1.026 Å.

3.3. DOS Functions of Chemisorption under Different Doping

To further understand the electronic structure characteristics of hydrogen adsorption surfaces under doped metals (Mn, Cr, Ni, Mo), we first imported the crystal structure model of α-Fe via MS, and optimized the model to ensure its accuracy. Subsequently, we carved out the (110) crystal plane from the optimized α-Fe crystal structure as the base surface for study, and introduced four different metal elements, Mn, Cr, Ni, and Mo, for doping. Following this, H atoms were introduced into these doped models, and placed at multiple possible adsorption sites for H atoms. Through continual experimentation and adjustments, stable adsorption models of H atoms on these doped surfaces were identified. Finally, we calculated the DOS functions by CASTEP, and the results are shown in Figure 5b,d,f,h,j. It can be observed that the DOS functions of hydrogen adsorption on a Fe surface doped with metals (Mn, Cr, Ni, Mo) are very similar to those of pure Fe surface. Furthermore, Fe s, p, and d orbitals on the undoped pure Fe surface and the s, p, and d orbitals of the dopant metal atoms hybridize with the s orbital of H, indicating the formation of chemical bonds between the doped metal atoms and H atoms. Among them, the doped metal elements contribute the most electrons on the d orbital. Compared with the Fe d orbital, the maximum peaks of the d orbital of Mn, Cr, and Mo shift to the right, in which Mo shifts the most, while Ni shifts to the left. After calculating the charge transfer values of H atoms on different surfaces, as shown in Figure 5k, we found that the doping of alloy elements reduced the absolute value of the charge transfer of H atoms, which inhibited the adsorption of hydrogen, which was mutually verified with the previous studies.

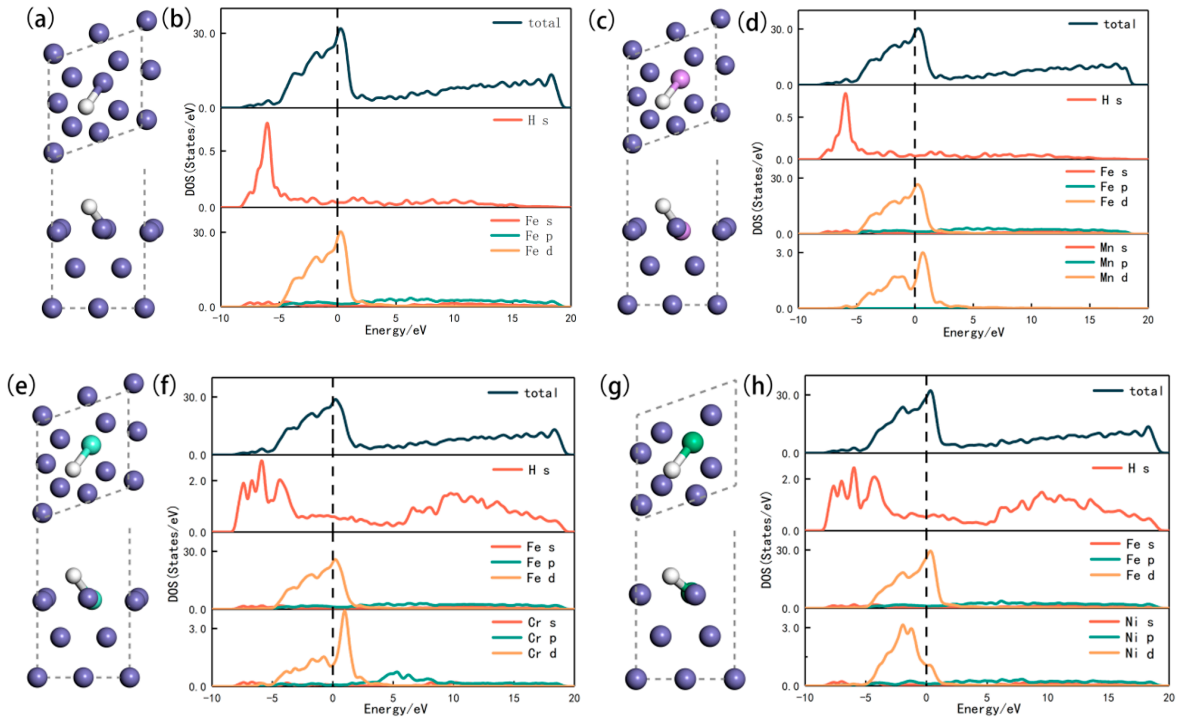

Figure 5. *Cont.*

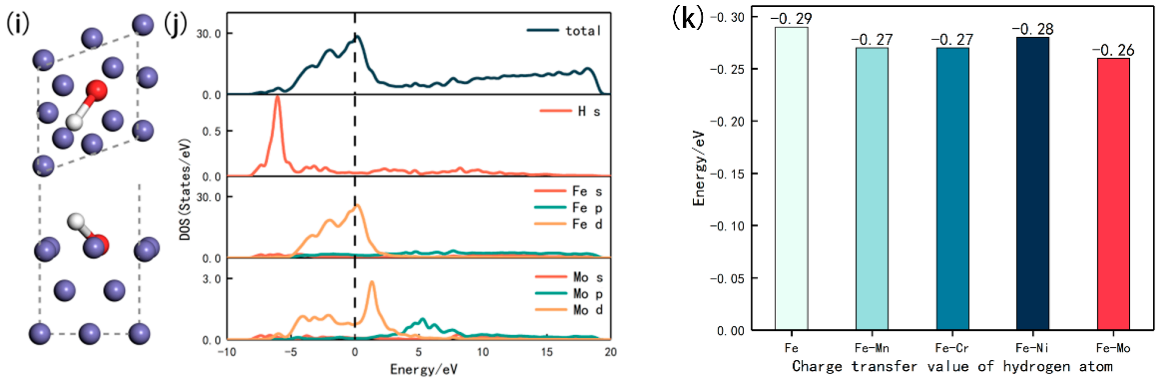

Figure 5. PDOS functions, (**a**) Fe surface hydrogen adsorption model, (**b**) Fe surface hydrogen adsorption DOS functions, (**c**) Fe/Mn surface hydrogen adsorption model, (**d**) Fe/Mn surface hydrogen adsorption DOS functions, (**e**) Fe/Cr surface hydrogen adsorption model, (**f**) Fe/Cr surface hydrogen adsorption DOS functions, (**g**) Fe/Ni surface hydrogen adsorption model, (**h**) Fe/Ni surface hydrogen adsorption DOS functions, (**i**) Fe/Mo surface hydrogen adsorption model, (**j**) Fe/Mo surface hydrogen adsorption DOS functions, (**k**) hydrogen atom charge transfer value.

3.4. Hydrogen Atom Diffusion under Different Doping

The energy required for the diffusion process of hydrogen atoms following the incorporation of each dopant is depicted in Figure 6f. As observed from Figure 6, the doping of Ni significantly promotes the diffusion of hydrogen atoms into the interior of the metal. In contrast, the addition of dopants such as Cr, Mn, and Mo serves to inhibit this diffusion. Specifically, the doping with Mn increases the energy required for hydrogen diffusion by a factor of 2.19, while Cr doping elevates this energy requirement to 20.25 times that of the undoped surface. Notably, among these, the doping of Mo demonstrates the most substantial hindering effect on hydrogen diffusion, with the energy required being 21.88 times greater than that of the undoped surface.

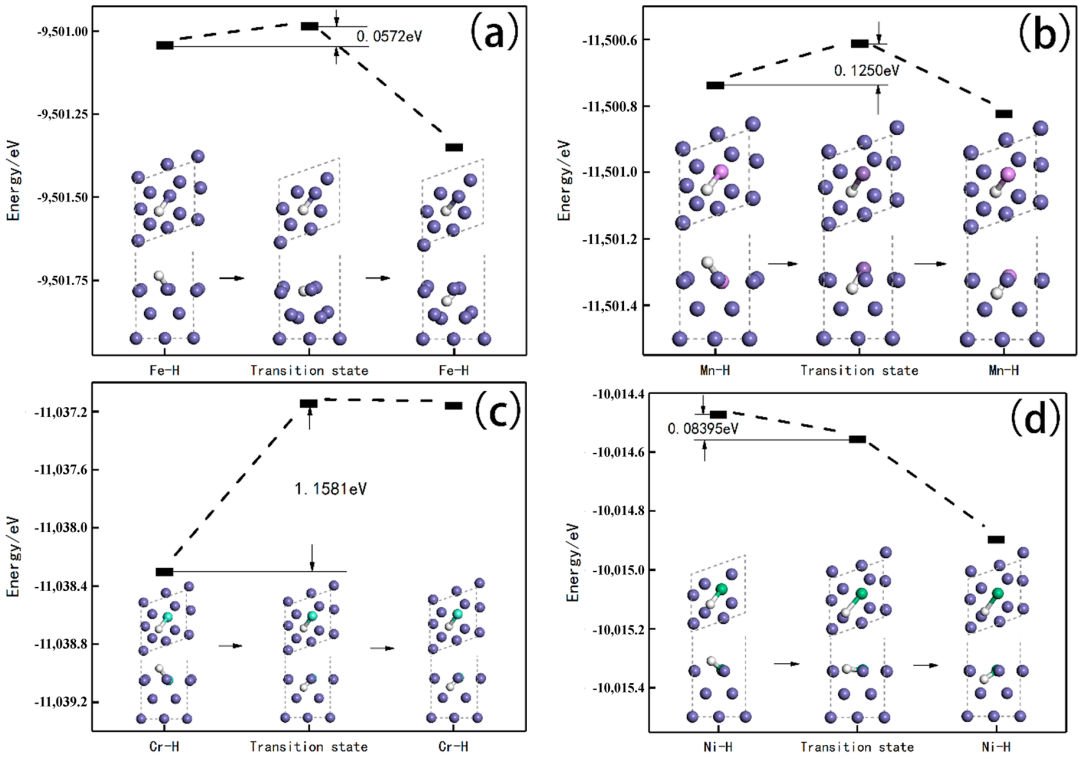

Figure 6. *Cont.*

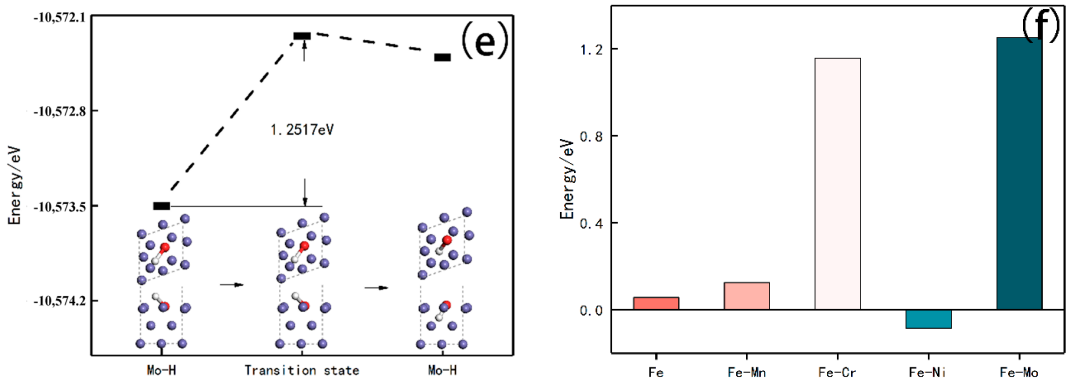

Figure 6. H atom diffusion process of different alloys: (**a**) H diffusion on Fe surface, (**b**) H diffusion on Fe/Mn surface, (**c**) H diffusion on Fe/Cr surface, (**d**) H diffusion on Fe/Ni surface, (**e**) H diffusion on Fe/Mo surface, and (**f**) energy required for diffusion on each surface.

4. Conclusions

In this paper, we used first principles calculations to analyze the adsorption and diffusion of hydrogen on Fe(110) surfaces doped with four different metals: Mn, Cr, Ni, and Mo. By calculating the adsorption energy, performing LST/QST transition state searches, and analyzing the electronic state densities on Fe(110) surfaces doped with Mn, Cr, Ni, and Mo, we compared these properties to those on pure Fe surfaces regarding the adsorption and diffusion of hydrogen. The adsorption energy of hydrogen atoms on the pure Fe surface was found to be −4.7606 eV. After doping with Mn, Cr, Ni, and Mo, the adsorption energies changed to −4.6828 eV, −4.6769 eV, −4.4798 eV, and −4.4566 eV, respectively. Doping with Mo resulted in the highest adsorption energy, thereby indicating that Mo doping has the strongest capability to inhibit the adsorption of hydrogen atoms. This is consistent with the bond length measurements, where Mo doping leads to the greatest distance between the hydrogen atoms and the surface at 1.026 Å. According to the charge transfer values of hydrogen atoms under different doping conditions, Mo doping most significantly impedes the charge transfer from hydrogen atoms to the metal. In the study of the energy barriers for hydrogen atom diffusion into the metal, it was found that Ni doping facilitates the diffusion of hydrogen atoms into the interior of the metal, while Cr, Mn, and Mo doping hinder it. Among these, the effect of Mo is the most pronounced, with the energy required for diffusion being 21.88 times higher than that on undoped surfaces. The appropriate addition of Cr and Mo is beneficial in preventing the adsorption and diffusion of hydrogen, thereby avoiding the occurrence of hydrogen-induced cracking. This is helpful for the design of hydrogen transport pipelines.

Author Contributions: Conceptualization, L.Z.; methodology, L.Z.; software, L.Z. and Q.Z.; validation, Q.Z.; formal analysis, Y.L., C.Z. and Y.D.; investigation, L.Z., Q.Z., P.J., Y.L., C.Z. and Y.D.; resources, L.Z.; data curation, Q.Z., Y.L., C.Z. and Y.D.; writing—original draft preparation, L.Z. and Q.Z.; writing—review and editing, Q.Z., P.J., Y.L., C.Z. and Y.D.; visualization, P.J.; supervision, L.Z.; project administration, L.Z.; funding acquisition, P.J. All authors have read and agreed to the published version of the manuscript.

Funding: This work was supported by the Hainan Provincial Key Research and Development Program under Grant ZDYF2023GXJS014, and the Heilongjiang Provincial Natural Science Foundation under Grant LH2022E029.

Data Availability Statement: The raw data supporting the conclusions of this article will be made available by the authors upon request.

Conflicts of Interest: The authors declare no conflicts of interest.

References

1. Ott, B.; Delafontaine, L.; Welchert, N.A.; Dee, S.; Reza, A. Ensuring natural gas infrastructure is suitable for hydrogen service. *Process Saf. Prog.* **2023**, *42*, 213–224. [CrossRef]
2. Bae, D.S.; Baek, U.B.; Nahm, S.H.; Jo, I. Effect of electrochemical hydrogen charging time on hydrogen embrittlement of the hot-rolled and accelerated cooling treated API X70 steel. *Met. Mater. Int.* **2022**, *28*, 466–474. [CrossRef]
3. Bolobov, V.I.; Latipov, I.U.; Popov, G.G.; Buslaev, G.V.; Martynenko, Y.V. Estimation of the Influence of Compressed Hydrogen on the Mechanical Properties of Pipeline Steels. *Energies* **2021**, *14*, 6085. [CrossRef]
4. Di Lullo, G.; Oni, A.O.; Kumar, A. Blending blue hydrogen with natural gas for direct consumption: Examining the effect of hydrogen concentration on transportation and well-to-combustion greenhouse gas emissions. *Int. J. Hydrogen Energy* **2021**, *46*, 19202–19216. [CrossRef]
5. Liu, B.; Liu, S.; Guo, S.; Zhang, S. Economic study of a large-scale renewable hydrogen application utilizing surplus renewable energy and natural gas pipeline transportation in China. *Int. J. Hydrogen Energy* **2020**, *45*, 1385–1398. [CrossRef]
6. Zhou, D.; Wang, C.; Yan, S.; Yan, Y.; Guo, Y.; Shao, T.; Li, T.; Jia, X.; Hao, J. Dynamic modeling and characteristic analysis of natural gas network with hydrogen injections. *Int. J. Hydrogen Energy* **2022**, *47*, 33209–33223. [CrossRef]
7. Liu, J.; Teng, L.; Liu, B.; Han, P.; Li, W. Analysis of hydrogen gas injection at various compositions in an existing natural gas pipeline. *Front. Energy Res.* **2021**, *9*, 685079. [CrossRef]
8. Cerniauskas, S.; Jose Chavez Junco, A.; Grube, T.; Robinius, M.; Stolten, D. Options of natural gas pipeline reassignment for hydrogen: Cost assessment for a Germany case study. *Int. J. Hydrogen Energy* **2020**, *45*, 12095–12107. [CrossRef]
9. Meng, B.; Gu, C.; Zhang, L.; Zhou, C.; Li, X.; Zhao, Y.; Zheng, J.; Chen, X.; Han, Y. Hydrogen effects on X80 pipeline steel in high-pressure natural gas/hydrogen mixtures. *Int. J. Hydrogen Energy* **2017**, *42*, 7404–7412. [CrossRef]
10. Nguyen, T.T.; Bae, K.O.; Jaeyeong, P.; Nahm, S.H.; Baek, U.B. Damage associated with interactions between microstructural characteristics and hydrogen/methane gas mixtures of pipeline steels. *Int. J. Hydrogen Energy* **2022**, *47*, 31499–31520. [CrossRef]
11. Cho, L.; Kong, Y.; Speer, J.G.; Findley, K.O. Hydrogen Embrittlement of Medium Mn Steels. *Metals* **2021**, *11*, 358. [CrossRef]
12. Galliano, F.; Andrieu, E.; Cloué, J.-M.; Odemer, G.; Blanc, C. Effect of temperature on hydrogen embrittlement susceptibility of alloy 718 in Light Water Reactor environment. *Int. J. Hydrogen Energy* **2017**, *42*, 21371–21378. [CrossRef]
13. Park, H.; Moon, B.; Moon, Y.; Kang, N. Hydrogen stress cracking behaviour in dissimilar welded joints of duplex stainless steel and carbon steel. *Metals* **2021**, *11*, 1039. [CrossRef]
14. Gaude-Fugarolas, D. Hydrogen Transport and Metal Embrittlement Risk in Storage and Industrial Applications. *Defect Diffus. Forum* **2019**, *397*, 141–146. [CrossRef]
15. Staykov, A.; Yamabe, J.; Somerday, B.P. Effect of hydrogen gas impurities on the hydrogen dissociation on iron surface. *Int. J. Quantum Chem.* **2014**, *114*, 626–635. [CrossRef]
16. An, T.; Zhang, S.; Feng, M.; Luo, B.; Zheng, S.; Chen, L.; Zhang, L. Synergistic action of hydrogen gas and weld defects on fracture toughness of X80 pipeline steel. *Int. J. Fatigue* **2019**, *120*, 23–32. [CrossRef]
17. Feng, C.; Peng, Z.; Li, X.; Bao, S.; Jiang, X. Ductile Fracture Prediction of X80 Pipeline Steel Using Void Growth Model. *Metals* **2022**, *12*, 923. [CrossRef]
18. Mondal, B.C.; Dhar, A.S. Burst pressure assessment of corroded pipelines using fracture mechanics criterion. *Eng. Fail. Anal.* **2019**, *104*, 139–153. [CrossRef]
19. Cauwels, M.; Depraetere, R.; De Waele, W.; Hertelé, S.; Depover, T.; Verbeken, K. Influence of electrochemical hydrogenation parameters on microstructures prone to hydrogen-induced cracking. *J. Nat. Gas Sci. Eng.* **2022**, *101*, 104533. [CrossRef]
20. Wasim, M.; Djukic, M.B. Hydrogen embrittlement of low carbon structural steel at macro-, micro- and nano-levels. *Int. J. Hydrogen Energy* **2020**, *45*, 2145–2156. [CrossRef]
21. Eliaz, N.; Banks-Sills, L.; Ashkenazi, D.; Eliasi, R. Modeling failure of metallic glasses due to hydrogen embrittlement in the absence of external loads. *Acta Mater.* **2004**, *52*, 93–105. [CrossRef]
22. Lynch, S. Hydrogen embrittlement phenomena and mechanisms. *Corros. Rev.* **2012**, *30*, 105–123. [CrossRef]
23. Matsumoto, R.; Taketomi, S.; Matsumoto, S.; Miyazaki, N. Atomistic simulations of hydrogen embrittlement. *Int. J. Hydrogen Energy* **2009**, *34*, 9576–9584. [CrossRef]
24. Sofronis, P.; Robertson, I.M. Transmission electron microscopy observations and micromechanical/continuum models for the effect of hydrogen on the mechanical behaviour of metals. *Philos. Mag. A* **2002**, *82*, 3405–3413. [CrossRef]
25. Takakuwa, O.; Mano, Y.; Soyama, H. Increase in the local yield stress near surface of austenitic stainless steel due to invasion by hydrogen. *Int. J. Hydrogen Energy* **2014**, *39*, 6095–6103. [CrossRef]
26. Vink, T.J.; Gijzeman, O.; Geus, J.W. CO interaction with Fe(100): Effects of carbon and oxygen adlayers on co adsorption isotherms. *Surf. Sci.* **1985**, *150*, 14–23. [CrossRef]
27. Benziger, J.; Madix, R.J. The effects of carbon, oxygen, sulfur and potassium adlayers on CO and H_2 adsorption on Fe(100). *Surf. Sci.* **1980**, *94*, 119–153. [CrossRef]
28. Merrill, P.B.; Madix, R.J. Hydrogen bonding on iron: Correlation of adsorption and desorption states on Fe(100) and perturbation of the Fe-H bond with coadsorbed CO. *Surf. Sci.* **1996**, *347*, 249–264. [CrossRef]
29. Sorescu, D.C. First principles calculations of the adsorption and diffusion of hydrogen on Fe(100) surface and in the bulk. *Catal. Today* **2005**, *105*, 44–65. [CrossRef]

30. Yu, M.; Liu, L.; Wang, Q.; Jia, L.; Hou, B.; Si, Y.; Li, D.; Zhao, Y. High coverage H_2 adsorption and dissociation on fcc Co surfaces from DFT and thermodynamics. *Int. J. Hydrogen Energy* **2018**, *43*, 5576–5590. [CrossRef]
31. Álvarez-Falcón, L.; Viñes, F.; Notario-Estévez, A.; Illas, F. On the hydrogen adsorption and dissociation on Cu surfaces and nanorows. *Surf. Sci.* **2016**, *646*, 221–229. [CrossRef]
32. Yanachkov, B.; Lyutov, L.; Katzarov, I.; Drenchev, L.; Kolev, K. Effect of Microstructure on the Mechanical Response of Hydrogen-Charged Pure Iron. *Metals* **2022**, *12*, 2160. [CrossRef]
33. Zhang, S.; Li, K.; Ma, Y.; Bu, Y.; Liang, Z.; Yang, Z.; Zhang, J. The Adsorption Mechanism of Hydrogen on FeO Crystal Surfaces: A Density Functional Theory Study. *Nanomaterials* **2023**, *13*, 2051. [CrossRef] [PubMed]
34. Dadfarnia, M.; Martin, M.L.; Nagao, A.; Sofronis, P.; Robertson, I.M. Modeling hydrogen transport by dislocations. *J. Mech. Phys. Solids* **2015**, *78*, 511–525. [CrossRef]
35. Ferrin, P.; Kandoi, S.; Nilekar, A.U.; Mavrikakis, M. Hydrogen adsorption, absorption and diffusion on and in transition metal surfaces: A DFT study. *Surf. Sci.* **2012**, *606*, 679–689. [CrossRef]
36. Xie, W.; Peng, L.; Peng, D.; Gu, F.L.; Liu, J. Processes of H_2 adsorption on Fe(110) surface: A density functional theory study. *Appl. Surf. Sci.* **2014**, *296*, 47–52. [CrossRef]
37. Chohan, U.K.; Jimenez-Melero, E.; Koehler, S.P.K. Surface atomic relaxation and magnetism on hydrogen-adsorbed Fe(110) surfaces from first principles. *Appl. Surf. Sci.* **2016**, *387*, 385–392. [CrossRef]
38. Dudek, P.; Piwowońska, J. Influence of Titanium on the Microstructure and Mechanical Properties of Foundry Zinc Alloy. *J. Mater. Eng. Perform.* **2022**, *31*, 9029–9038. [CrossRef]
39. Feldshtein, E.E.; Dyachkova, L.N.; Patalas-Maliszewska, J. On Investigating the Microstructural, Mechanical, and Tribological Properties of Hybrid FeGr1/SiC/Gr Metal Matrix Composites. *Materials* **2021**, *14*, 174. [CrossRef]
40. Ning, Y.; Fu, M.W.; Hou, H.; Yao, Z.; Guo, H. Hot deformation behavior of Ti–5.0Al–2.40Sn–2.02Zr–3.86Mo–3.91Cr alloy with an initial lamellar microstructure in the $\alpha + \beta$ phase field. *Mater. Sci. Eng. A* **2011**, *528*, 1812–1818. [CrossRef]
41. Wu, Q.; Li, S. Alloying element additions to Ni3Al: Site preferences and effects on elastic properties from first-principles calculations. *Comput. Mater. Sci.* **2012**, *53*, 436–443. [CrossRef]
42. Xiang, C.; Liu, Y.; Liu, B.; Ca, O.Y.; Gan, Z. Characterization of hot deformation behavior of Ti–3Al–5Mo–4.5V alloy with a martensitic starting microstructure. *J. Micromechanics Mol. Phys.* **2017**, *2*, 1750011. [CrossRef]
43. Liu, G.; Chen, H.; Gao, W.; Huang, Z.; Yang, Y.; Li, Z.; Yan, M.; Fu, Y.-D. First-principles analysis on the nitrogen adsorption and diffusion in Ti alloy towards clarified diffusion mechanism in nitriding. *J. Mater. Res. Technol.* **2022**, *21*, 1479–1489. [CrossRef]
44. Stenczel, T.K.; El-Machachi, Z.; Liepuoniute, G.; Morrow, J.D.; Bartók, A.P.; Probert, M.I.J.; Csányi, G.; Deringer, V.L. Machine-learned acceleration for molecular dynamics in CASTEP. *J. Chem. Phys.* **2023**, *159*, 044803. [CrossRef]
45. White, J.A.; Bird, D.M. Implementation of gradient-corrected exchange-correlation potentials in Car-Parrinello total-energy calculations. *Phys. Rev. B Condens. Matter* **1994**, *50*, 4954–4957. [CrossRef] [PubMed]
46. Zou, L.; Wang, Z.; Zong, Z. Generalized differential transform method to differential-difference equation. *Phys. Lett. A* **2009**, *373*, 4142–4151. [CrossRef]
47. Broyden, C.G. The Convergence of a Class of Double-rank Minimization Algorithms: 2. The New Algorithm. *IMA J. Appl. Math.* **1970**, *6*, 222–231. [CrossRef]
48. Mayorga, R.V.; Quintana, V.H. A family of variable metric methods in function space, without exact line searches. *J. Optim. Theory Appl.* **1980**, *31*, 303–329. [CrossRef]